

## Identifying Transients in the Dark Energy Survey using Convolutional Neural Networks

 VENKITESH AYYAR,<sup>1,2</sup>  ROBERT KNOP JR.,<sup>1</sup>  AUTUMN AWBREY,<sup>1,3</sup>  ALEXIS ANDERSEN,<sup>1,3</sup> AND  
 PETER NUGENT<sup>1,3</sup>

<sup>1</sup>*Lawrence Berkeley National Laboratory, 1 Cyclotron Rd, Berkeley, CA, 94720, USA*

<sup>2</sup>*Hariri Institute for Computing and Computational Science and Engineering, Boston University, Boston, MA, 02215, USA*

<sup>3</sup>*Department of Astronomy, University of California, Berkeley, Berkeley, CA, 94720, USA*

### Abstract

The ability to discover new transients via image differencing without direct human intervention is an important task in observational astronomy. For these kind of image classification problems, machine Learning techniques such as Convolutional Neural Networks (CNNs) have shown remarkable success. In this work, we present the results of an automated transient identification on images with CNNs for an extant dataset from the Dark Energy Survey Supernova program (DES-SN), whose main focus was on using Type Ia supernovae for cosmology. By performing an architecture search of CNNs, we identify networks that efficiently select non-artifacts (e.g. supernovae, variable stars, AGN, etc.) from artifacts (image defects, mis-subtractions, etc.), achieving the efficiency of previous work performed with random Forests, without the need to expend any effort in feature identification. The CNNs also help us identify a subset of mislabeled images. Performing a relabeling of the images in this subset, the resulting classification with CNNs is significantly better than previous results.

*Keywords:* –Dark Energy Survey –Type Ia supernovae –Convolutional Neural Networks –Random Forest

### 1. INTRODUCTION

A major aspect of observational astronomy is the “survey” which involves the wholesale mapping of various regions of the sky to create catalogs which are subsequently mined for scientifically important astronomical objects. While most astronomical phenomena occur over very large time scales, of the order of millions of years, certain phenomena occur over much shorter time scales spanning minutes to a few months and may either be static, and thus changing in brightness, or moving across the sky. Telescope images of such events are generically labeled as astrophysical transients. Some examples of such transients are solar system objects, supernovae, active galactic nuclei, variable stars, and neutron star mergers, etc. Since some of these events are quite rare and will fade rapidly, it is often important to trigger follow-up observations immediately (additional photometry, spectroscopy, etc.) to glean their underlying nature and discover new physics. Hence, identifying transients in images quickly and efficiently is very important so as not to waste precious, and expensive, follow-up resources.

For many years this process was conducted by manual inspection of images by humans. However, given the magnitude of image data generated by modern telescopes, it become imperative to automate this process via machine Learning techniques. This was first done by the SNFactory (Bailey et al. 2007) where boosted decision trees were employed to greatly reduce the number of candidates. Subsequently, Bloom et al. (2012) took it to the next level using random forests to mine the Palomar Transient Factory data for new transients. Surveys such as the Dark Energy Survey (DES) Flaugher (2005) map the sky both on a large scale and deeply, producing up to 170GB of raw imaging data every night.

In this work, we describe our efforts to perform transient identification in DES. This work builds on previous work with random forest Goldstein et al. (2015); Mahabal et al. (2019); Wright et al. (2015) to classify Type Ia supernova from other Artifacts of processing and instrumentation for the DES-SN data. Machine learning techniques such as

Convolutional Neural networks (CNNs) have shown remarkable success in image classification problems. Here we apply these to identify transient Supernova images. We are aware of one prior work with CNNs for transient identification<sup>1</sup>.

After giving a brief description of CNNs in Section 2, we describe our dataset in Section 3. In Section 4, we discuss our procedure and present our results. Finally, we summarize our findings in Section 5. Our code is available at the [github repository](#)<sup>2</sup>.

## 2. CONVOLUTIONAL NEURAL NETWORKS

Here we give a brief introduction to convolutional neural networks. *Neural networks* are machine learning computing systems that are very efficient at learning patterns in input data. These are generic functions consisting of weight parameters organized in layers. Acting on the input data, after periodic application of non-linear *activation* functions, they produce outputs which can be either numbers (for regression) or class labels (for classification). By minimizing the deviation between computed output and the expected output, one arrives at the optimal weight parameters. The procedure to compute the weights of a network is called *training the network*. A properly trained network learns the generic function and can correctly predict the outputs for an unseen dataset. Essentially, they are universal function approximators.

Convolutional neural networks are a class of neural networks that specialize in recognizing patterns in image data. Using blocks of kernels that scan through the images, they extract features at different scales. Figure 2 gives the general layout of a CNN. A typical CNN is made up of the following basic layers:

- **Convolution layers:** These perform convolutional operations on the images to extract feature maps.
- **Subsampling layers:** Operating on feature maps, the subsampling layers compress the dimensionality to reduce the number of parameters.
- **Fully connected layers:** These layers combine different features of a single layer together.

CNNs typically have very large number of parameters and hence are prone to overfitting. One way to mitigate this is by using dropout layers that help suppress the unimportant weights by setting weight parameters to zero during training.

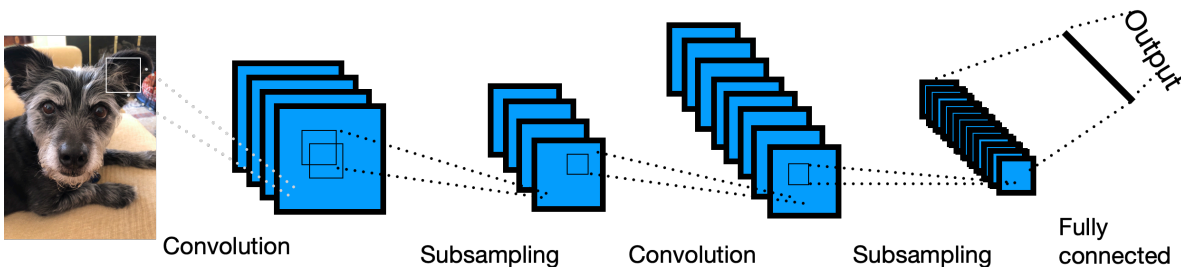


**Figure 1.** The general structure of a CNN with *convolution*, *subsampling* and *fully connected* layers.

CNNs have been used extensively for image recognition, classification for images obtained both in the real world and in scientific experiments. Large multi-layered Neural networks, despite having large number of free parameters have shown remarkable success in image classification. Nevertheless, many studies have used specialized CNNs that have connections between non-adjacent layers such as *Resnet* He et al. (2015) and *Unet* Ronneberger et al. (2015). In a previous work (Ayyar et al. 2020), we found that instead of using CNNs with a few but long layers, CNNs with a reasonably high number of layers with fewer parameters were remarkably successful in classifying signal from background for datasets in high energy physics experiments. This prompted us to explore the potential of such layered *deep* CNNs for classification problems in astronomy.

<sup>1</sup> Previous work using CNN's on DES data can be found [here](#)

<sup>2</sup> We provide the best saved models and notebooks for plotting and visualization [here](#)

### 3. DATASET

#### 3.1. Dataset

We used the same dataset used in [Goldstein et al. \(2015\)](#). The data collected is from the August 2013 through February 2014 of DES science operations and consists of 898,963 independent samples. Each sample in turn consists of 3 types of 2D images of dimension  $51 \times 51$ . The 3 types are labelled: *Template*, *Search*, and *Difference*. To incorporate the information from all 3 images, we use them as channels. In other words, each input sample is a 3 channel image of dimensions  $51 \times 51$ , having an expected label: Artifact (1) or Non-Artifact(0). Due to the original timing of the data collection, it lacked non-artifact sources. Hence, the original authors used the method of artificial source construction, and thus injected these non-artifacts into the images. This method has been used extensively before [Bailey et al. \(2007\)](#) [Bloom et al. \(2012\)](#). For this dataset, all non-artifacts were artificially generated.

Figure 2 depicts the three channels for 5 independent samples for both artifacts and non-artifacts. Distinguishing them visually requires some level of expertise. A more detailed explanation of the dataset can be found in [Goldstein et al. \(2015\)](#).

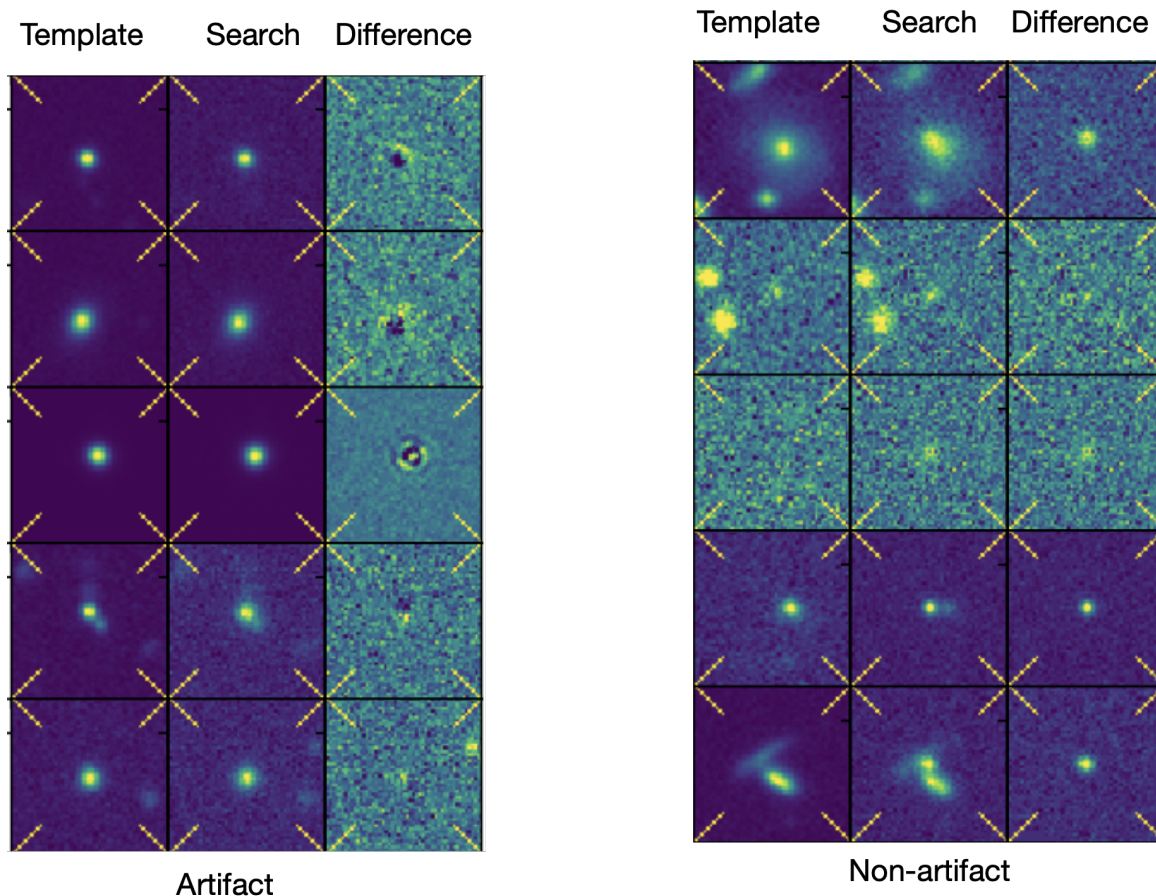


**Figure 2.** The figure shows the three channels: template, search and difference for 5 different artifact and non-artifact samples.

#### 3.2. Classification and ROC curves

In classification problems, the model provides a class prediction for each sample. The aim is to develop a model that categorizes most samples correctly. For a binary classification problem like this one, the performance can be summarized by a  $2 \times 2$  confusion matrix shown in Figure 3. Some common classifier performance metrics are the True Positive Rate (TPR), False Positive Rate (FPR) and Missed Detection Rate (MDR). They are defined as:

$$MDR = \frac{F_n}{T_p + F_n}$$

		True Labels	
		Non-artifact (label=0)	Artifact (label=1)
Predicted Labels	Non-artifact (label=0)	$T_p$ True positive	$F_p$ False positive
	Artifact (label=1)	$F_n$ False negative	$T_n$ True negative

**Figure 3.** The Confusion matrix for a binary classifier.

$$\begin{aligned}
 FPR &= \frac{F_p}{F_p + T_n} \\
 TPR &= \frac{T_p}{T_p + F_n}
 \end{aligned} \tag{1}$$

where the quantities  $T_p$ ,  $T_n$ ,  $F_p$  and  $F_n$  are defined in Figure 3. Since the classifier prediction is a floating point number between 0 and 1, one uses a *threshold* parameter to determine a predicted class. The behavior of the classifier as threshold is varied, can be seen through the Receiving Operator Characteristic (ROC) curve. The ROC curve is the most commonly used method to compare a set of classifier models. A useful quantity used for comparison of models is the Area Under the Curve (AUC), which is expected to approach 1.

## 4. ANALYSIS AND RESULTS

### 4.1. CNN architecture search

The goal of this work was to develop optimized CNNs by exploring various CNN architectures. Starting with 4-5 different CNN architectures, we performed variations in kernel sizes, dropout layer locations and dropout ratios, types of pooling, learning rates, etc., and compared the classification performance of these models. Picking the best performing models among these, we performed further modifications and compared their performance. We performed a few such iterations, studying about 100 different CNN models in total. We found 4 models with completely different architectures that achieved good performance.

### 4.2. Results with original labels

For the first part of the work, we split the data into *Training* (50%), *validation* (5%) and *test* samples (5%). The validation data was used to assess the classification performance of trained models on unseen data. The test data was used to compare the ROC curves of the different models. At this stage, we kept about 40% of the data in reserve for further analysis. We also trained a random forest using the hyperparameters described in the Goldstein et al. (2015).

Table 1 compares the four best CNN models. All models have an AUC score close to 1.0. Figure 4 shows the FPR-MDR ROC curve for the best CNN models. The black squares represent the ROC curve of the random forest from Figure 7 of Goldstein et al. (2015). Here we see that our CNN models and the random forest are comparable in performance to the previous work.

Figure 5 shows the prediction histogram for Model 1. Noting the log-scale on the y-axis, it is clear that most of the samples are classified correctly as either artifacts or non-artifacts. Also, very few samples have prediction scores in the

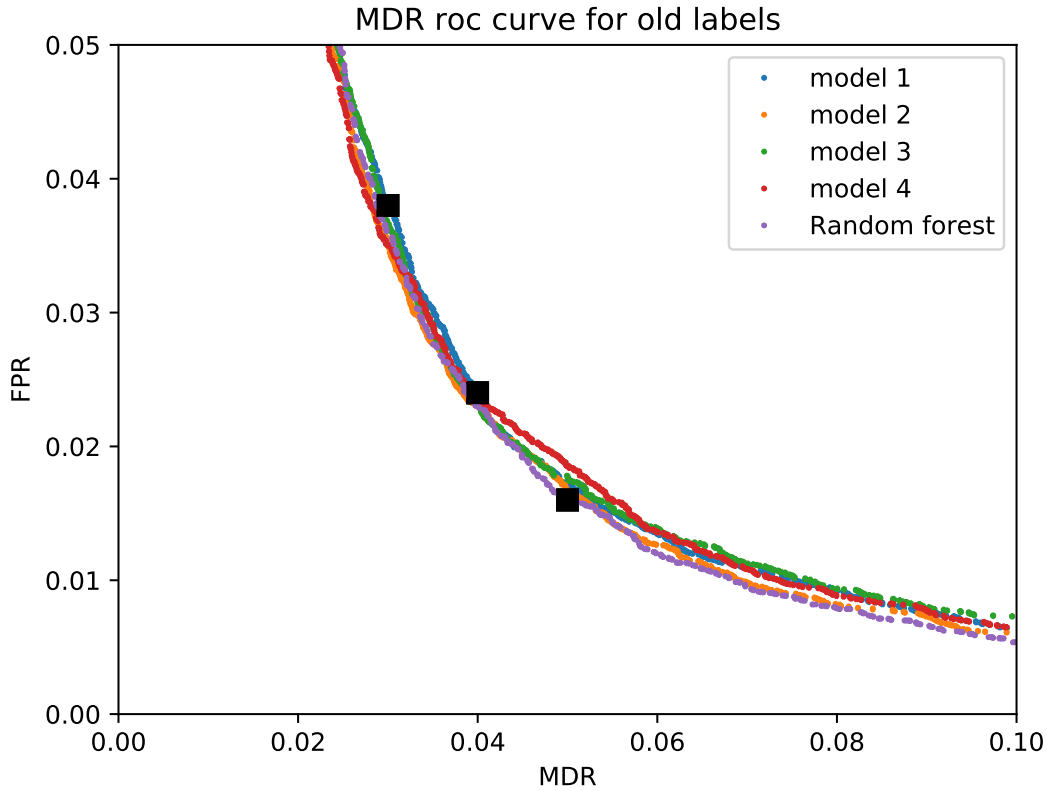


**Figure 4.** The ROC curve of FPR vs MDR for the CNN models. The black squares show the points obtained in the previous paper with a random forest. The ROC curves of all the models are adjacent to each other implying similar classification performance.

Model name	Number of parameters	Area under curve (AUC)	Training time per epoch on GPU
1	266k	0.994	60s
2	415k	0.994	127s
3	853k	0.993	190s
4	954k	0.994	47s

**Table 1.** Table describing the best performing CNN models.

intermediate 0.2-0.8 range, which is the hallmark of a good classifier. The prediction histograms for the other three models also look very similar.

#### 4.3. *Mislabeled images*

Since the CNNs use the entire information from the images, one would expect well trained CNNs to achieve optimal classification performance. While the CNNs in Figure 4 do perform very well, the fact that they do not improve upon the performance of the random forest, prompted us to explore their classification in more detail.

In the bottom left part of Figure 5, it can be seen that a significant number of artifacts with input label 1 are accorded a prediction value very close to 0. Similarly, a large number of non-artifacts with input label 0 have prediction values close to 1, as seen in the bottom right. We see a similar pattern for the other CNN models. This seems to imply that the CNN models are strongly mis-classifying a few samples, thus affecting the quality of their ROC curves.

To better understand this issue of strong mis-classification, we divided the samples into 6 categories depending on the original label and the predicted value for the model. For example, category 1 corresponds to samples that are labeled as artifacts (label=1), but have prediction values between 0 and 0.1. We then compare the number of samples in the

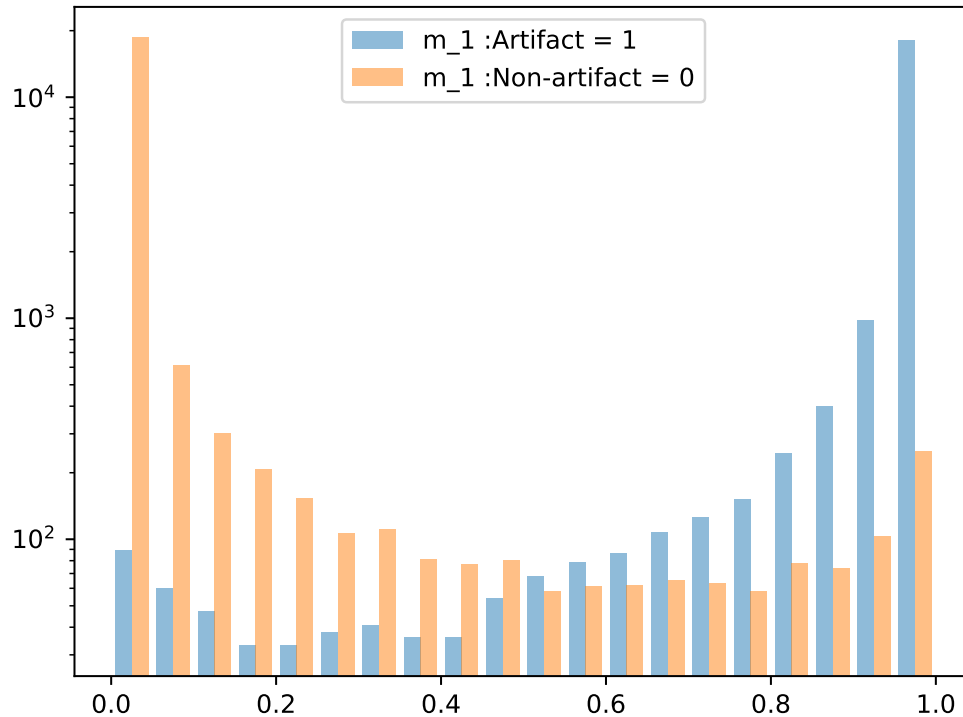


**Figure 5.** The prediction histograms for Model 1. Note the log scale on the y-axis. Most of the labels are predicted correctly. Also, there are relatively very few predictions in the intermediate region.

different categories for the different models. The results and description of the categories are summarized in Table 2. It can be seen that the CNN models have more points in categories 1 and 6, corresponding to strongly mis-classified samples.

Category	Original Label	Prediction range	Description	Model 1	Model 3	Random Forest
1	1	0-0.1	Strongly mis-classified Artifact	0.35 %	0.76 %	0.15 %
2	1	0.1-0.5	Weakly mis-classified Artifact	0.9 %	1.2 %	1.0 %
3	1	0.5-1.0	Correctly classified Artifact	48.2 %	47.7 %	48.4 %
4	0	0 - 0.5	Correctly classified Non-artifact	48.4 %	49 %	48.4 %
5	0	0.5 - 0.9	Weakly mis-classified Non-artifact	1.2 %	0.8 %	1.6 %
6	0	0.9 - 1.0	Strongly mis-classified Non-artifact	0.8 %	0.7 %	0.4 %

**Table 2.** Dividing the samples into categories, depending on model predictions. Categories 1 and 6 correspond to the strongly mis-classified samples. The CNN models have more strongly mis-classified samples.

To better understand this, we look at how the samples classified by Model 1 into category 1 are categorized by other models. In Figure 6, we show histograms of prediction values for the other 3 models and random forest, for 149 samples that were classified by Model 1 to be in category 1. It can be seen that about 66% of the points are also placed in category 1 by the other 3 CNN models. However, the random forest model places only about 25 % of these points in category 1. A similar pattern is seen for samples in Category 6 as well, as shown in Figure 7. This is further confirmation that the four CNN models seem to strongly mis-classify the same set of images.

#### 4.4. Relabeling

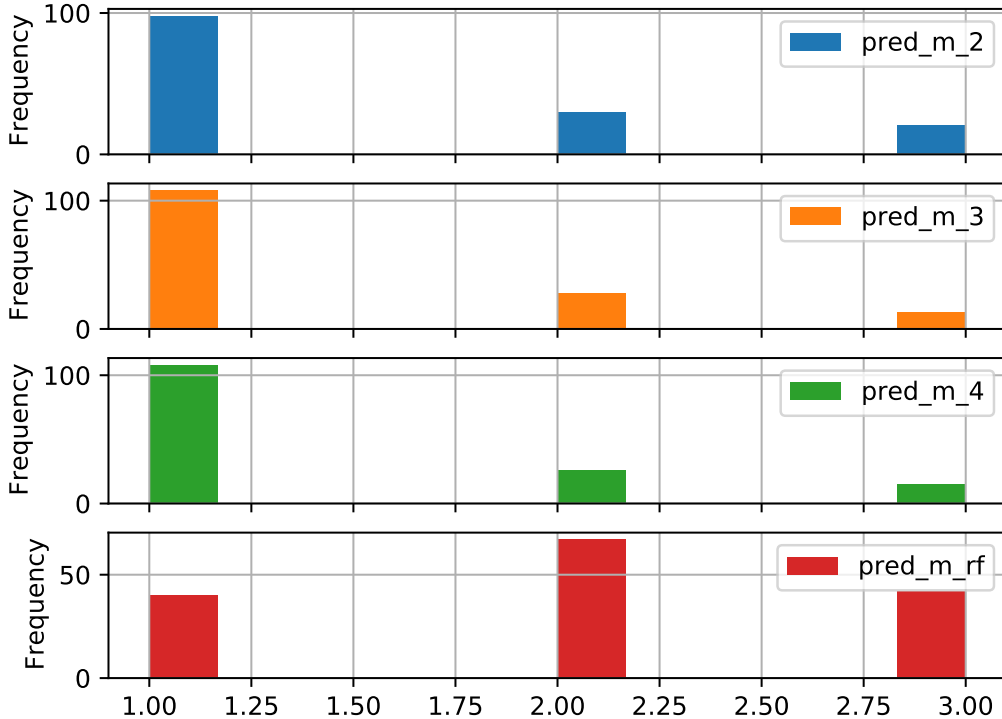


**Figure 6.** The figure shows how the different models categorize the 149 samples of a test dataset that are in category 1 for Model 1. The CNNs place about 66% of these samples in category 1. The random forest places only 25% of these, instead placing many of the rest in category 2.

The fact that different optimally trained CNN models strongly mis-categorize the same set of samples, points to the possibility of a case of mislabeling. To confirm this, we went back to the set of images in categories 1 and 6 for Model 1. Upon performing a visual inspection for a small subset of these samples, we found that about 90% of these samples were indeed given the wrong label during the process of data preparation. As the artifact sample was randomly drawn from all detections, while the non-artifact came from injected transient candidates this is not too surprising. In fact, what we saw in our visual inspection is that some of the injected non-artifacts fell on bad parts of the CCD detector or were located near saturated stars while several of the artifacts were in fact heretofore unknown astrophysical transients.

For the purposes of relabeling, we developed a GUI tool in python using the *Tkinter* library that enabled us to view blocks of images with their labels and allow an expert to quickly mark the images that require relabeling. As a first step, we performed a relabeling of roughly 750 samples that were classified into categories 1 and 6 by Model 1. Using the same trained models and their predictions, and just using the new labels, the resulting ROC curves are shown in Figure 8. It is clear that the models are doing significantly better with the newer labels. In addition, the CNN models are now performing better than the random forest. This implies that despite all models being trained with a dataset containing some mislabeled points, the CNNs are doing a better job at classification.

Having convinced ourselves of the efficacy of the relabeling process, we then obtained the predictions of Model 1 on the entire dataset. Then, collecting the samples in categories 1 and 6, we then performed a relabeling of this set. We found that the relabeling changed the labels of roughly 80% of the roughly 8000 samples that we reviewed.

#### 4.5. Results with new labels

We trained all four CNN models and the random forest on the relabeled dataset, after splitting the data into training (70%), validation (10%), and test samples (20%). The resulting ROC curves are shown in Figure 9. It is clear

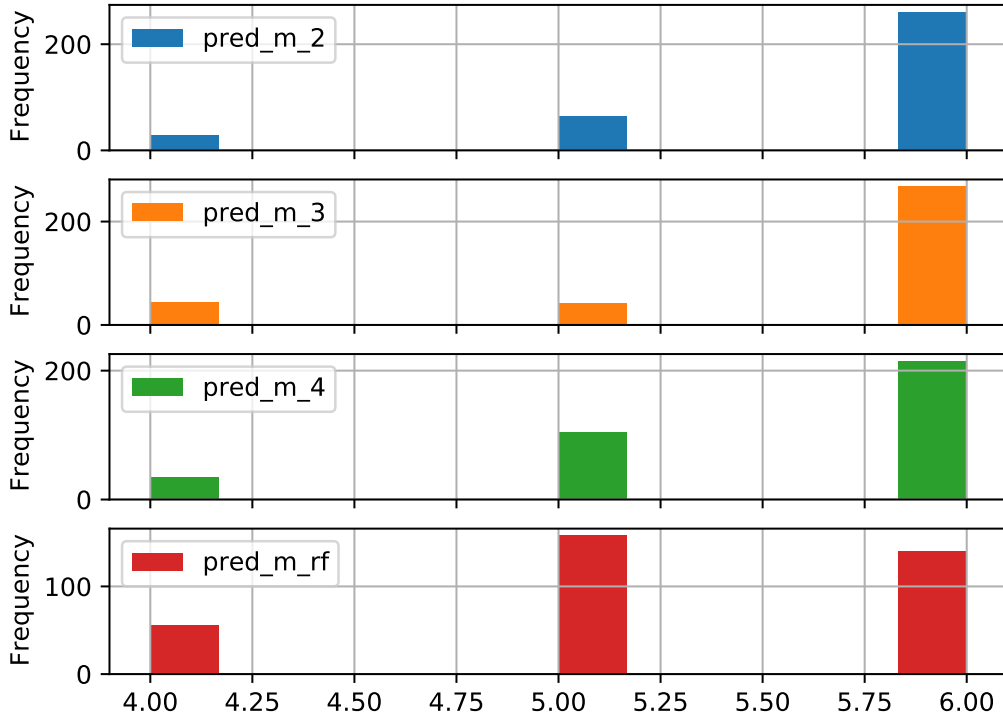


**Figure 7.** The figure shows how the different models categorize the 354 samples of a test dataset that are in category 6 for Model 1. The CNNs place about 66% of these samples in category 6. The random forest places only 40% of these, instead placing many of the rest in category 5.

Layer	Output Shape	No. of Parameters
Input	$51 \times 51 \times 3$	0
Conv2D	$51 \times 51 \times 80$	2240
BatchNorm	$51 \times 51 \times 80$	320
MaxPooling	$25 \times 25 \times 80$	0
Conv2D	$25 \times 25 \times 80$	57680
BatchNorm	$51 \times 25 \times 25$	320
MaxPooling	$12 \times 12 \times 80$	0
Conv2D	$12 \times 12 \times 80$	57680
BatchNorm	$12 \times 12 \times 80$	320
MaxPooling	$6 \times 6 \times 80$	0
Flatten	2880	0
Dropout	2880	0
Dense	51	146931
BatchNorm	51	204
Dense	1	52
Total trainable parameters		<b>265,165</b>

**Table 3.** The structure of the best chosen CNN model: Model 1.

that the random forest is performing better with the new, relabeled dataset, and the four CNN are comparable in



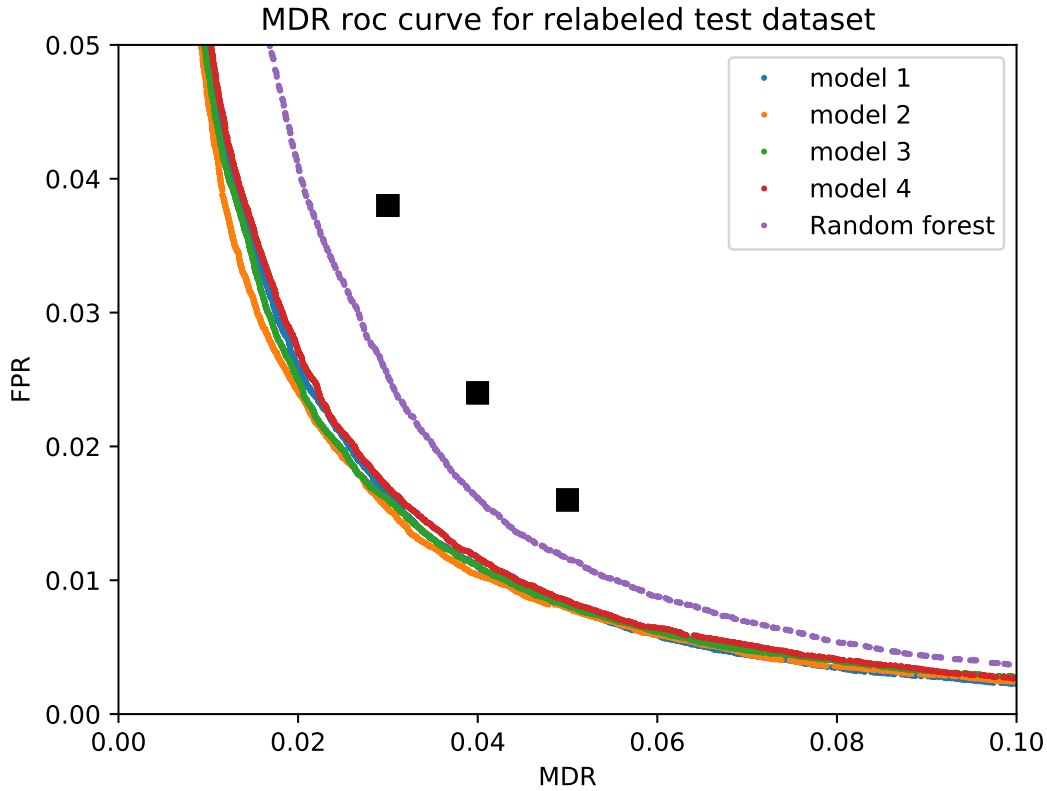


**Figure 8.** The ROC curve of FPR vs MDR for the previously trained models using new labels for the test dataset. The black squares show the points obtained in the previous paper with random forest. The CNN models and random forest show significant improvement.

Category	1: Train and test with old labels	2: train with old labels, test with new labels	3: train-test with new labels
1	0.35 %	0.2 %	0.36 %
2	0.75 %	0.82 %	0.83 %
3	48.4 %	49 %	49.1 %
4	48.4 %	48.8 %	48.5 %
5	1.2 %	1.02 %	0.77 %
6	0.84 %	0.23 %	0.33 %

**Table 4.** Comparing the points in various categories for the three cases:

1: Train and test with old labels, 2: train with old labels, but test with new labels, 3: train and test with new labels. Comparing columns 1,2 and 3, it can be seen that column 2 has few points in Categories 1 and 6, since the test dataset was biased by Model 1. Column 3 has slightly higher values in these categories compared to column 2, since the models were re-trained on a bigger dataset. Overall, column 3 has fewer points in Category 6 than 1, implying that the relabeling procedure had the intended effect.

performance, but better than the random forest. Figure 4.5 shows the ROC comparing the true positive rate with the false positive rate as defined in Eqn 1. Based on the two ROC curves, we choose Model 1 as our best model, although the classification of the four CNN models are fairly similar. We present the learning curve of Model 1 in Figure 11 and its detailed structure in Table 3.

It might be argued that our relabeling process might be biasing the performance of Model 1, since we chose the points to relabel, based on the predictions of Model 1. However, in Section 4.2, we trained with only 50% of the samples, keeping the rest of the data in reserve. For this final analysis, we built the dataset with a different random

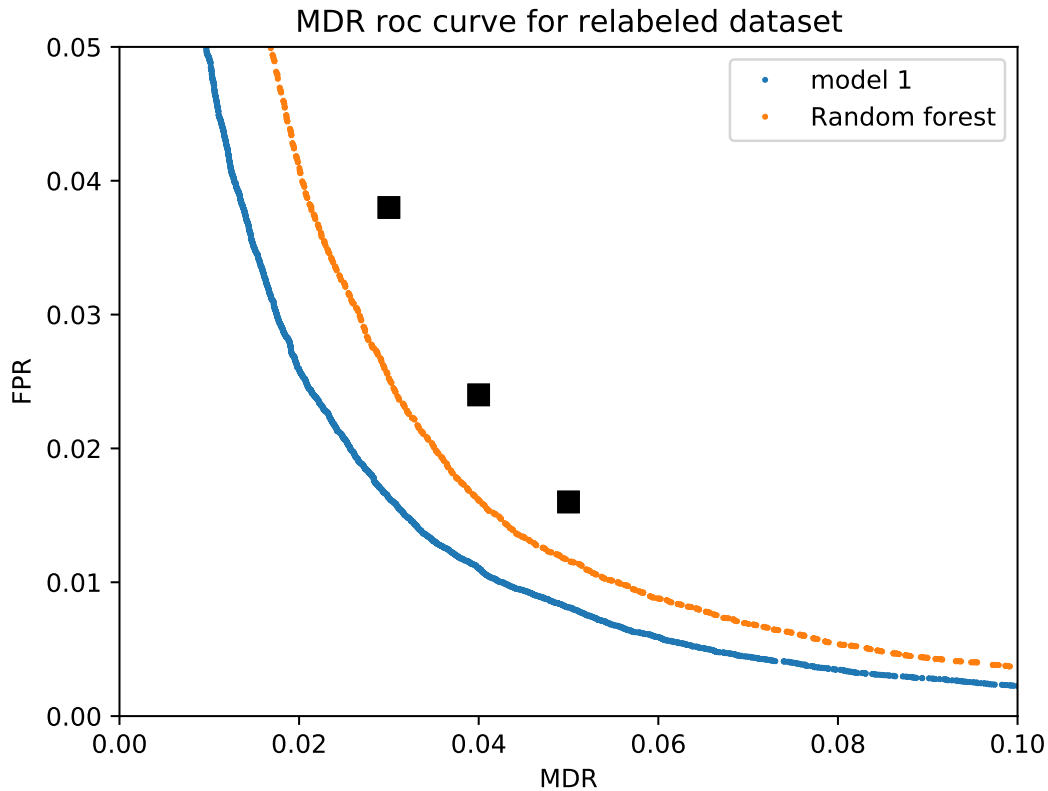


**Figure 9.** The ROC curves of the best chosen CNN model: model 1 and random forest that were trained on the relabeled dataset. The black squares show the points obtained in the previous paper with the random forest. It is clear that Model 1 outperforms the random forest even on the relabeled dataset.

seed and used 70% of the data for training, thus mitigating the bias. Table 4 shows the number of points in various categories for Model 1 for the three cases: train-test with old labels, train with old label, test with new labels, train and test with new labels. It is clear that values in column 2 are lowest, due to the bias. But the values in column 3 are intermediate, indicating that the bias has been mitigated. Hence, we are confident that our final CNN models are indeed better at classification than the random forest.

#### 4.6. Results in an ongoing survey

We are currently using the CNN to provide a real/bogus score for an ongoing survey, the DECam Deep Drilling Fields (DDF) program. This is being run at the Blanco 4m telescope at Cerro Tololo-Inter-American Observatory as part of the DECam Alliance for Transients (DECAT), a consortium of time-domain DECam programs<sup>3</sup>. Because this is real, incoming data, we don't have the absolute truth as to what's a genuine transient and what's a subtraction artifact or other "bogus" event, as we would in the case of a simulation. To evaluate the performance of the model, several observers manually tagged over 20,000 events as "real" or "bogus". In this way, we're testing the actual "autoscan" behavior of the CNN, it's ability to substitute for manual vetting by observers of objects detected on difference images. We found that the performance of the model trained for this paper was not great on this data set. In particular, there was a fairly high missed detection rate (MDR), reaching 0.5 depending on the real/bogus cutoff used. A visual inspection of a subset of these missed detections showed that many were marginal (either low signal-to-noise or possible, but not obvious, subtraction artifacts near the cores of objects visible on the template image).

To allow the CNN to better model the visual scanning of this survey, we re-trained the model using the data from this survey. We included detections that had been vetted by at least 3 observers, using the majority for a real/bogus

<sup>3</sup> The ongoing Graham et al. program is described [here](#)

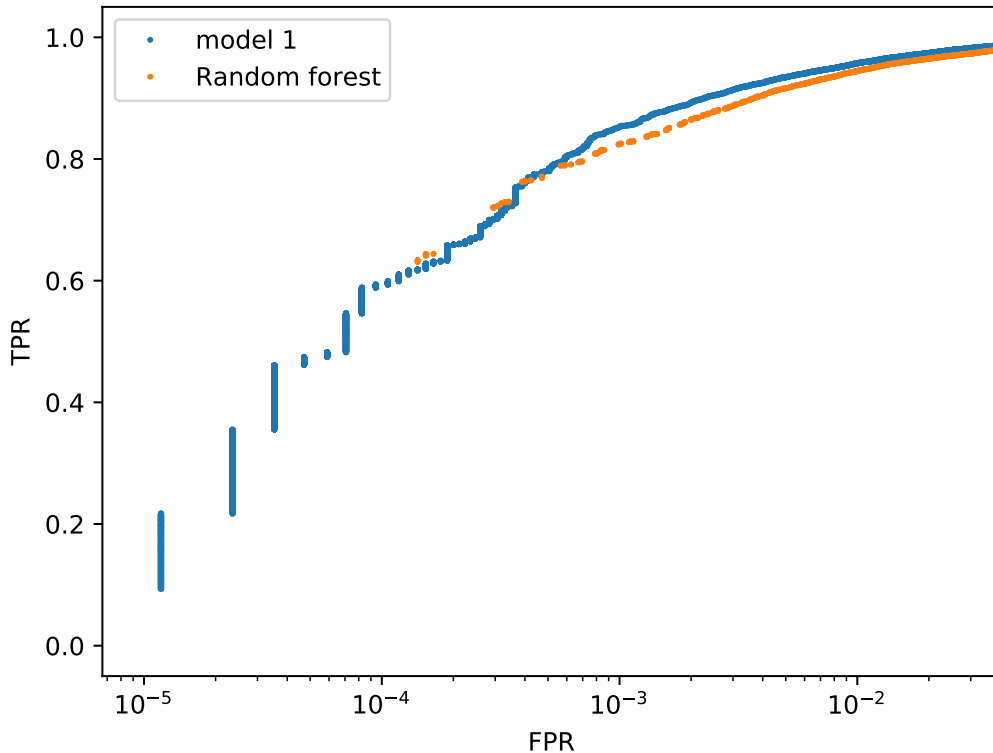


**Figure 10.** The figure shows the ROC curves for Model 1 and random forest, plotting the true positive rate (TPR) with the false positive rate (FPR).

classification. For this dataset, about 15% of the detections were good. This retrained model performed much better than the original model on this new dataset; results are shown in Figures 12 and 13. We cannot expect the ROC curve (left plot of Figure 12 here to be as good as the ones in Figure 9 because the input data set is not nearly as clean; we don't know what are really good events, and in practice trained observers will disagree in some cases about what is a good vs. a bogus detection.

Thus, the model obtained using a CNN architecture optimized for the original dataset works fairly well with another, similar dataset, after a re-training of the weights. This points to our model architecture being fairly generic and hence more broadly applicable for datasets of this type. To improve upon the performance on this new dataset, we would have to perform another architecture search with a subset of this new data. We aim to address this in a future publication.

## 5. CONCLUSIONS AND DISCUSSION

### 5.1. Inference

We have discussed automating the identification of transient detections obtained in astronomical imaging data using machine learning. Here we developed CNN models trained directly on the raw image data. The best CNN models match the performance of the previously used random forest method. In addition, using the CNNs predictions, we were able to identify that some of the images were mislabeled in the original data. After performing a relabelling of 1% of the dataset, we re-trained the best CNN models. The resultant models outperform the original random forest method. We also find that the CNNs are more robust to mislabeled samples in the training data.

Since we have only relabeled a small subset of the data (1%), there is still the possibility that many other points are mislabelled. However, the significant increase in classification performance suggests that we have identified and relabelled most of the mislabeled images.

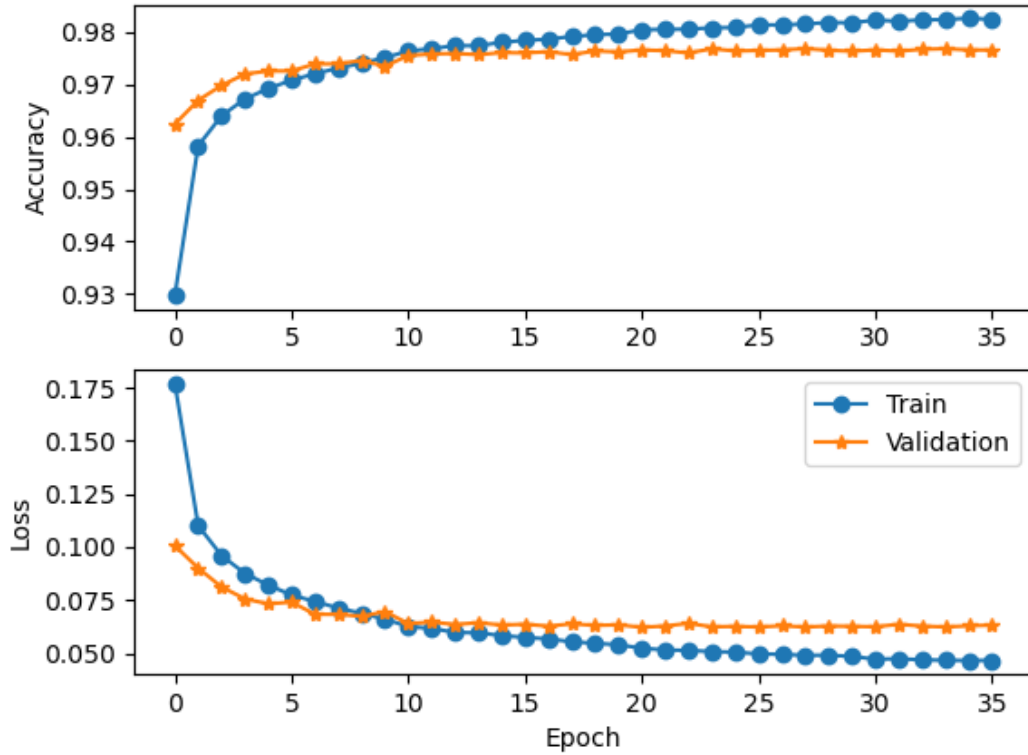


**Figure 11.** The figure shows the learning curves for CNN Model 1. The top figure provides the training and validation accuracy values at the end of each epoch, while the bottom figure provides the corresponding loss values. The validation loss and accuracy stabilize after about 10 epochs.

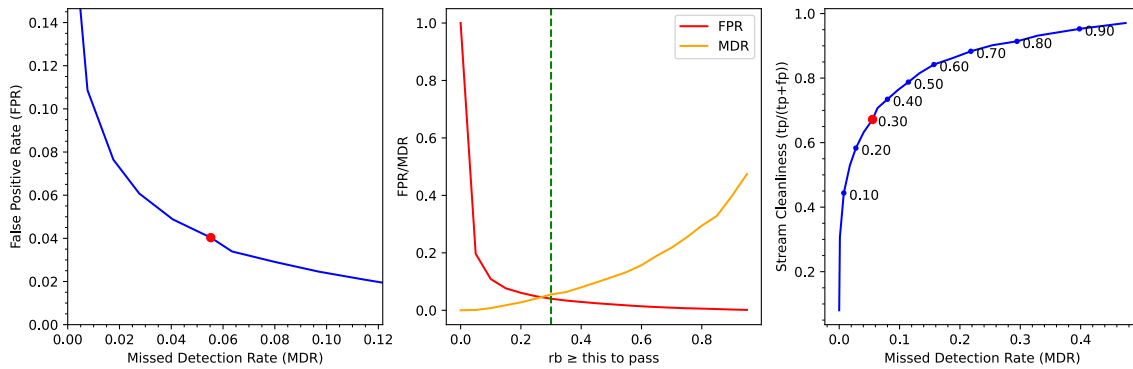


**Figure 12.** Results for the CNN model trained against manual vetting of the ongoing DECAT/DDF survey. Left: ROC curve. Middle: false positive rate (FPR) and missed detection rate (MDR) as a function of real/bogus score cutoff. Right: stream cleanliness vs. MDR. Stream cleanliness is the fraction of passed objects that are real objects. This is different from  $1 - \text{FPR}$  because in the real dataset, there are a factor of 6 more bogus events than real events. In the left and right plots, the red dot indicates the chosen real/bogus threshold of 0.3 that will be used in determining if an alert should be sent out for the detection. The dashed green vertical line in the middle plot is the same cutoff.

## 5.2. Discussion

There are two main benefits of using CNNs over random forest for image classification: classification efficiency and ease of use.

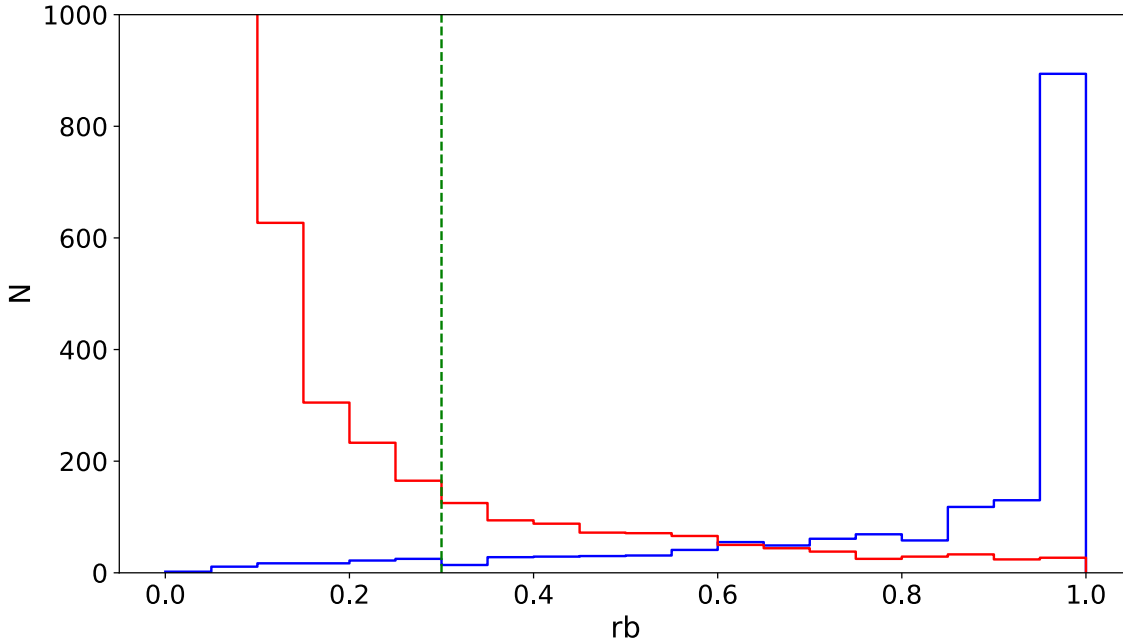


**Figure 13.** Histogram of real/bogus produced by the CNN for the ongoing DECAT/DDF survey. The blue histogram are events labelled as "real" by at least two out of three visual inspections, and the red histogram are events labelled as "bogus". The vertical dashed green line is the real/bogus threshold of 0.3 that will be used for generating alerts. Compared to Figure 5; as discussed in the text, we cannot expect the histogram to be as cleanly separated with this dataset as we can for the dataset used for the bulk of the paper.

Currently in astronomy, random forest methods are the most common method to auto-identify transients in image subtractions. In [Wright et al. \(2015\)](#), the authors compared the performance of random forests with neural networks and demonstrated that their random forest was most efficient. However, in our work, we have demonstrated that our CNN, obtained by performing a detailed architecture search, outperforms our random forest. Since the datasets are different, one cannot perform a direct comparison of ROC curves. However, the fact that our CNN outperforms the our random forest on the same dataset clearly demonstrates the benefit of using CNNs.

Another benefit of CNNs is their ease of implementation. One of the drawbacks of the original random forest method is the need to identify a set of important features to use. This process is fairly painstaking, and also involves performing many, often computationally expensive, operations on the raw images. The CNN method, on the other hand works directly on the raw image data. Although it requires an architecture search, different models with reasonably high complexity perform well in classification. Their computational cost is also quite reasonable as they run efficiently on GPUs. Hence, we believe the CNN method is more suitable for implementing automation of image subtraction classification in astronomy. Such methods could, and should, be explored in upcoming transient surveys such as the Rubin Observatory ([Street et al. 2020](#)) and the La Silla Schmidt Southern Survey (Nugent et al., in prep.) among others.

#### ACKNOWLEDGEMENTS

The entire code was written in python and keras, using jupyter notebooks for visualizations [Kluyver et al. \(2016\)](#). This research used resources of the National Energy Research Scientific Computing Center (NERSC), a U.S. Department of Energy Office of Science User Facility operated under Contract No. DE-AC02-05CH11231. V.A.'s work was supported by the Computational Center for Excellence, a Computational HEP program in the Department of Energy's Science Office of High Energy Physics (Grant #KA2401022). P.E.N. and R.A.K. acknowledge support from the DOE under grant DE-AC02-05CH11231, Analytical Modeling for Extreme-Scale Computing Environments.

#### REFERENCES

- Ayyar, V., Bhimji, W., Gerhardt, L., Robertson, S., & Ronaghi, Z. 2020, in 24th International Conference on Computing in High Energy and Nuclear Physics. <https://arxiv.org/abs/2002.05761>
- Bailey, S., Aragon, C., Romano, R., et al. 2007, *Astrophys. J.*, 665, 1246, doi: [10.1086/519832](https://doi.org/10.1086/519832)
- Bloom, J., et al. 2012, *Publ. Astron. Soc. Pac.*, 124, 1175, doi: [10.1086/668468](https://doi.org/10.1086/668468)
- Flaugher, B. 2005, *International Journal of Modern Physics A*, 20, 3121, doi: [10.1142/S0217751X05025917](https://doi.org/10.1142/S0217751X05025917)
- Goldstein, D. A., D'Andrea, C. B., Fischer, J. A., et al. 2015, *The Astronomical Journal*, 150, 82, doi: [10.1088/0004-6256/150/3/82](https://doi.org/10.1088/0004-6256/150/3/82)
- He, K., Zhang, X., Ren, S., & Sun, J. 2015, *CoRR*, abs/1512.03385. <https://arxiv.org/abs/1512.03385>
- Kluyver, T., Ragan-Kelley, B., Pérez, F., et al. 2016, in *Positioning and Power in Academic Publishing: Players, Agents and Agendas*, ed. F. Loizides & B. Schmidt, IOS Press, 87 – 90
- Mahabal, A., Rebbapragada, U., Walters, R., et al. 2019, *Publications of the Astronomical Society of the Pacific*, 131, 038002, doi: [10.1088/1538-3873/aaf3fa](https://doi.org/10.1088/1538-3873/aaf3fa)
- Ronneberger, O., Fischer, P., & Brox, T. 2015, *CoRR*, abs/1505.04597. <https://arxiv.org/abs/1505.04597>
- Street, R. A., Bianco, F. B., Bonito, R., et al. 2020, *Research Notes of the American Astronomical Society*, 4, 41, doi: [10.3847/2515-5172/ab812a](https://doi.org/10.3847/2515-5172/ab812a)
- Wright, D. E., Smartt, S. J., Smith, K. W., et al. 2015, *Monthly Notices of the Royal Astronomical Society*, 449, 451, doi: [10.1093/mnras/stv292](https://doi.org/10.1093/mnras/stv292)